Memo M and P No. 67

AN EXPLANATION OF THE APPARENT BRIDGMAN EFFECT IN MERCHANT'S ORTHOGONAL CUTTING RESULTS

P.L.B. Oxley* and M.J.M. Welsh*

Abstract

In Merchant's modified shear angle solution it is assumed following Bridgman that the shear strength of the work material is a function of the hydrostatic stress. Although Merchant's experimental results confirm the assumed relation subsequent workers have failed to obtain such agreement. In this paper it is shown that Merchant's results can be explained independently of the Bridgman effect by considering the variable flow stress properties of the work material, which are strain-rate dependent.

*The College of Aeronautics, Cranfield, Bedford, England.

Introduction

In orthogonal cutting the tool cutting edge is parallel to the newly machined surface and perpendicular to the cutting direction. If the depth of cut (t in Fig. 1) is small compared with the width of cut, then the removed chip is formed under approximately plane strain conditions. If the chip is formed by plastic flow without fracture and there is no build-up of work material on the cutting tool, then the process is approximately a steady state process.

By taking cine films through a microscope of the side of cut while cutting it has been shown that under the above conditions the chip is formed in a plastic zone of the shape shown in Fig. 1. The chip is curled and only contacts the tool over a short length before curling away from the tool face. If there are no forces on the clearance face of the tool, then the tool-work force system can be represented as in Fig. 2. The resultant cutting force is transmitted across the tool-chip interface, through the plastic zone and into the work and can conveniently be resolved into various sets of components. Considering the tool-chip interface, the components shown represent the friction force F and normal force N acting between the chip and tool. It is usual to represent the frictional condition at the tool-chip interface by a mean friction angle λ (Fig. 2) where λ is given by

$$\tan \lambda = \frac{F}{N} \qquad (1)$$

For the plastic zone the resultant can be resolved into shear and normal components on a plane such as AB (Fig. 2). The resultant can also be resolved into components in the direction of cutting F_c and normal to this

direction F_t. These are the forces normally measured in cutting tests and can be used to calculate λ from the relationship

$$\tan (\lambda - \alpha) = \frac{F_t}{F_c} \qquad (2)$$

where α (Fig. 1) is the tool rake angle.

In analysing orthogonal cutting it is usual to assume that chip formation can be represented as shown in Fig. 3, with the chip formed by simple shear across a single shear plane AB. The velocity gradient across the chip and the resulting chip curl are neglected. For a given depth of cut t and rake angle α the geometry of Fig. 3 is not completely defined unless either the chip thickness T or the shear angle ϕ (i.e. the angle between the shear plane AB and the direction of cutting) is known. A number of equations for predicting ϕ have been proposed and probably the best known of these is that due to Merchant (1), namely

$$\phi = \frac{\pi}{4} + \frac{\alpha}{2} - \frac{\lambda}{2} \qquad (3)$$

Merchant obtained this equation by expressing the force in the direction of cutting F_c (Fig. 2) in terms of ϕ, α, λ and t and the shear strength of the work material, which he assumed was constant, and then selecting ϕ to make F_c a minimum. He carried out a series of cutting tests to check equation (3) using experimental cutting forces and equation (2) to calculate λ and experimental chip thickness ratios $(\frac{t}{T})$ and the equation

$$\tan \phi = \frac{\frac{t}{T} \cos \alpha}{1 - \frac{t}{T} \sin \alpha} \qquad (4)$$

to calculate ϕ. These results are reproduced in Fig. 4 and it can be seen

that equation (3) overestimates ϕ. This lack of agreement led Merchant to propose that the shear strength of the work material (i.e. shear stress along shear plane) would not be constant as assumed in deriving equation (3) but would be a function of the normal (hydrostatic) stress on the shear plane. Thus following the work of Bridgman he introduced the linear relationship

$$k = k_o + np_a \qquad (5)$$

where k is the shear stress along the shear plane and p_a is the average normal (hydrostatic) stress on the shear plane. Introducing equation (5) into the analysis and again selecting ϕ to make F_c a minimum he obtained the equation

$$2\phi = \cot^{-1}n + \alpha - \lambda \qquad (6)$$

where n is the slope in equation (5). In checking equation (6) Merchant did not measure n by an independent test e.g. combined torsion-axial compression test, but instead calculated k and p_a from his cutting results. These are reproduced in Fig. 5 and it can be seen that the experimental points follow a linear relationship fairly closely with n approximately equal to 0.23. The corresponding shear angle equation ($2\phi = 77 + \alpha - \lambda$) is shown in Fig. 4 and can be seen to be in good agreement with the experimental results.

Subsequent work (2) on different materials has not shown the same degree of agreement between cutting results and equations (5) and (6). Independent measurements (3) of equation (5) suggest that the values of n needed to satisfy cutting data are too large. This lack of agreement

between Merchant's modified theory and experiment is all the more disappointing when it is realized that this is one of the very few cutting theories in which account is taken of work material properties.

In this paper Merchant's results are reanalysed using a theory recently introduced by the authors (4) in which account is taken of the variable flow stress properties of the work material which are strain-rate dependent. The normal stress is shown to vary along the shear plane and the apparent relationship (in Merchant's results) between the average value of this stress and the shear stress is seen to result not from a Bridgman effect but from the variable flow stress properties.

Variable Flow Stress Theory

Let us assume: (1) that the work material is an isotropic, plastic-rigid material in which the flow stress can vary with strain-rate, strain-hardening, etc.; (2) that the removed chip is continuous without built-up edge and is formed under approximately plane strain conditions; (3) that the chip is formed in a shear zone which has straight parallel sides as shown in Fig. 6, with AB, CD and EF representing shear lines, i.e. directions of maximum shear stress and maximum shear strain-rate. It is implicit in this last assumption that the chip is straight and not curled and that the shear strain and shear stress are constant along each of the shear lines AB, CD and EF.

For a perfectly sharp tool the shear line AB (Fig. 6) will transmit the resultant cutting force and to satisfy equilibrium the resultant across AB must be equal in magnitude and must act along the same line as the resultant transmitted by the tool-chip interface. The stresses along

AB can be expressed in terms of the cutting conditions, material properties and Φ (the angle made by AB with the direction of cutting). From a geometrical viewpoint AB can be considered a shear plane, as in the Merchant (1) analysis, with Φ the shear angle. That is, experimental values of Φ can be calculated from equation (4).

For plane strain conditions the shear stress on AB is the shear flow stress k and the normal stress is the hydrostatic stress p. Consider the equilibrium of the small element of the shear zone shown in Fig. 7. As the material passes through the shear zone its shear flow stress will change, as a result of strain-hardening, temperature, etc. Therefore, let the shear flow stress along CD (i.e. initial shear flow stress at zero plastic strain) be $k - \frac{\Delta k}{2}$, and let the shear flow stress along EF be $k + \frac{\Delta k}{2}$. The total change in shear flow stress is then Δk. Resolving forces parallel to AB gives

$$\Delta p = \frac{\Delta k}{\Delta s_1} \Delta s_2 \qquad (7)$$

where Δp is the change in hydrostatic stress across the element, Δs_1 is the width of the shear zone and Δs_2 is measured along AB. According to this equation the hydrostatic stress along AB must vary for a material whose shear flow stress changes during cutting. Applying this equation between A and B and noting that $\frac{\Delta k}{\Delta s_1}$ is constant along AB we obtain

$$p_A - p_B = \frac{\Delta k}{\Delta s_1} \cdot \frac{t}{\sin \Phi} \qquad (8)$$

or

$$p_B = p_A - \frac{\Delta k}{\Delta s_1} \frac{t}{\sin \Phi}$$

where p_A is the hydrostatic stress at A (i.e. normal stress on AB at A) and p_B is the hydrostatic stress at B (i.e. normal stress on AB at B). For a constant value of $\frac{\Delta k}{\Delta s_1}$ along AB the variation in hydrostatic stress along AB will be linear and the total normal force per unit width acting on AB will be

$$F_N = \frac{p_A + p_B}{2} \quad \frac{t}{\sin \phi} \tag{9}$$

The corresponding shear force on AB will be

$$F_S = k \frac{t}{\sin \phi} \tag{10}$$

If then the angle made by the resultant cutting force with AB is θ (Fig. 6) we have

$$\tan \theta = \frac{F_N}{F_S} = \frac{p_A + p_B}{2k} \tag{11}$$

In a detailed analysis (5) of the plastic zone it was found that the hydrostatic stress in the region of A could be calculated most reliably from the free surface condition in the work material between C and A (Fig. 6), the free surface becoming cracked and therefore irregular between A and E. Consider a shear line $A_1A_2A_3B_1$ adjacent to AB as shown in Fig. 8, with A_3B_1 parallel to AB. In order to satisfy equilibrium $A_1A_2A_3B_1$ as a line of maximum shear stress must meet the free surface at 45° and the hydrostatic stress in the triangular zone A A_1A_2 must be equal to the shear flow stress in this region. From physical considerations this hydrostatic stress will be compressive. p_A can now be found by considering the equilibrium of the element A A_2A_3. Taking moments about A gives

$$p_A = k(1 + 2(\pi/4 - \phi)) \tag{12}$$

If p_A is known, then equation (8) can be used to calculate p_B. In this equation Δk is the change of shear flow stress occurring in the shear zone. If we idealize the shear flow stress-shear strain curve of the work material as shown in Fig. 9 then

$$\Delta k = m\gamma \tag{13}$$

where m is the slope of the plastic stress-strain curve at the corresponding mean shear strain rate in the shear zone and γ is the shear strain along EF (Fig. 6). Before this equation can be used it is necessary to know the mean shear strain rate in the shear zone $\dot{\gamma}_{mean}$ and also the shear strain γ.

The maximum shear strain rate $\dot{\gamma}_{max}$ (i.e. the shear strain rate in the direction of the shear lines AB, CD, and EF) can be expressed in the usual way in terms of the velocities of flow, that is,

$$\dot{\gamma}_{max} = \sqrt{\left(\frac{\partial u}{\partial y} + \frac{\partial v}{\partial x}\right)^2 + 4\left(\frac{\partial u}{\partial x}\right)^2} \tag{14}$$

where u and v are the velocities in the x and y directions respectively (Fig. 10). To calculate the mean (maximum) shear strain rate in the shear zone we can consider a single finite step and measure Δu, Δv, Δx and Δy as shown in Fig. 10, that is,

$$\Delta u = \frac{-U \cos\alpha \cos\phi}{\cos(\phi - \alpha)}$$

$$\Delta v = \frac{U \cos\alpha \sin\phi}{\cos(\phi - \alpha)} \tag{15}$$

$$\Delta x = \Delta s_1 / \sin\phi$$

$$\Delta y = \Delta s_1 / \cos\phi$$

where Δs_1 is the width of the shear zone and U is the work velocity. Substituting these values in equation (14) gives

$$\dot{\gamma}_{mean} = \frac{U \cos \alpha}{\Delta s_1 \cos(\phi - \alpha)} \tag{16}$$

or if U is in f.p.m. and Δs_1 is in in.

$$\dot{\gamma}_{mean} = \frac{0.2\ U \cos \alpha}{\Delta s_1 \cos(\phi - \alpha)} \text{ per sec.} \tag{17}$$

The shear strain along EF can be found by multiplying the mean shear strain rate by the time a particle takes to cross the shear zone. This gives

$$\gamma = \frac{\cos \alpha}{\sin \phi \cos(\phi - \alpha)} \tag{18}$$

It is now possible to calculate the stress distribution along AB and hence θ (Fig. 6) for any value of ϕ provided that certain work material properties (e.g. slope m) and the size of the shear zone are known.

The angle θ can also be expressed in terms of the frictional condition along the tool chip-interface and if we follow the usual practice and represent this frictional condition by a mean angle of friction λ, then (see Fig. 2)

$$\theta = \phi + \lambda - \alpha \tag{19}$$

Before the above equations can be used some assumption must be made about the size of the shear zone. From the experimental work of Kececioglu (6) and Nakayama (7) at relatively high cutting speeds and of Enahoro (8) and Palmer and Oxley (5) at low cutting speeds it appears that the ratio of the length to mean width of the shear zone ($t/\Delta s_1 \sin \phi$) lies between 6 and 12 for a range of cutting conditions and work materials. Although this work

is far from conclusive, it would suggest that as a first step this ratio can be assumed constant. For the purpose of our calculations we will assume that

$$\frac{\dot{t}}{\Delta s_1 \sin \phi} = 10 \qquad (20)$$

For the work material the relation between the slope m and the shear strain rate, and between the initial shear flow stress and shear strain rate must be known. Although these are apparently fundamental work material properties and measurements of the variation of initial shear flow stress with strain rate have been made, the authors are not aware of similar measurements of the slope m over the required range of shear strain. In view of this curves of m and initial shear flow stress obtained by Oxley (9) from an analysis of Kececioglu's cutting results (6) were used by the authors in a previous paper (4) to calculate ϕ. These are given in Figs. (11) and (12) and it can be seen that the slope m decreases with increase in shear strain rate while the initial shear flow stress increases. For steel these are the expected trends.

In making calculations it was found most convenient to assume particular values of ϕ, for given conditions of rake angle, depth of cut and cutting speed, and then to work through the equations to find the corresponding values of mean friction angle λ. (A specimen calculation is given in an Appendix at the end of this paper.) Graphs of ϕ against $\lambda - \alpha$ can then be plotted in the usual way as shown in Fig. 13. It can be seen (Fig. 13) that the present theory is speed (strain-rate) sensitive and, for example, it is predicted that, for given cutting conditions, a decrease in speed will lead to a decrease in ϕ. It is well known that experiments confirm this trend.

Results and Discussion

Curves of slope m and initial shear flow stress for Merchant's work material (N.E.9445 steel) are shown dotted in Figs. 11 and 12. These were obtained by analysing cutting data by the method described by Oxley (9). The curves are very similar to those for Kececioglu's work material (SAE 1015), shown by the full lines in Figs. 11 and 12, the main difference being the higher values of shear flow stress for Merchant's material.

The variable flow stress theory has been used to calculate Φ for Merchant's cutting conditions (including experimental values of λ) and although there is some slight variation of Φ with depth of cut and cutting speed the result of these calculations can be represented by a sirgle line as shown in Fig. 14. The experimental values of Φ given in Fig. 14 show good agreement between theory and experiment.

Fig. 15 gives the values of p_a, the average normal (hydrostatic) stress on AB (i.e. $p_a = \frac{p_A + p_B}{2}$), and k, the shear flow stress on AB calculated from the variable flow stress theory for Merchant's cutting conditions (including experimental values of λ). The agreement between Fig. 15 and Merchant's results (Fig. 5) can be seen to be remarkably good. It is important to note that Fig. 15 is derived from the curves of m and initial shear flow stress and does not result from a Bridgman type relationship. There is no apparent reason why work materials should have variable flow stress properties which yield a similar linear relation between p_a and k and indeed cutting experiments (2) on different materials do not show such a relationship. It can also be expected from the variable flow stress theory

that had Merchant's tests covered a wider range of cutting conditions and, for example, included slow cutting speed tests then the linear relation of Fig. 5 would have no longer applied.

The variable flow stress theory can be criticised on the grounds that the m and initial shear flow stress curves are obtained by analysing cutting data and therefore that the agreement shown between theory and experiment (Fig. 14) is not surprising. Although agreeing that independent measurements of these curves are desirable we would argue that it is highly significant that a material's cutting characteristics can be described so affectively by two apparently fundamental curves which show the same trends, where comparison is possible, as shown by independent measurements. It is also worth pointing out that when one considers designing an independent test for measuring these curves at the relevant strain-rates and temperatures it seems quite possible that a carefully conducted cutting test (or very similar test) might be the only practical solution.

In conclusion it is of interest to calculate, using the variable flow stress theory, the specific cutting pressure for Merchant's cutting conditions; Merchant's results showing a marked size effect i.e. increase of specific cutting pressure with decrease in depth of cut. The specific cutting pressure is defined as the force in the direction of cutting (F_c in Fig. 2) divided by the area of cut and is given by

$$\text{specific cutting pressure} = \frac{k \cos(\lambda - \alpha)}{\sin \phi \cos(\phi + \lambda - \alpha)} \qquad (21)$$

Fig. 16 gives the results of these calculations together with Merchant's experimental values. The increase in specific cutting pressure results from

two main causes (a) the decrease in shear angle ϕ with decrease in depth and (b) the increase in shear strain rate (see equations (20) and (17)), which increases the shear flow stress (Fig. 12), with decrease in depth. It is usual to associate this size effect with the natural nose radius of the tool cutting edge which tends to reduce the effective tool rake angle with decrease in depth. The above analysis suggests that a size effect can be expected even with a 'perfectly' sharp tool.

Acknowledgements

The authors wish to thank Professor J. Loxham for his help and encouragement and Production Tool Alloy Co. Ltd., for their support of one of the authors.

Appendix - Specimen Calculation

Consider the following cutting conditions:

rake angle α = 10°

depth of cut t = 0.008 in.

cutting speed U = 100 f.p.m.

Assume ϕ = 25°

from Eqn. (20) Δs_1 = 0.0019 in.

From Eqn. (17) $\dot{\gamma}$ = 10700 per sec.

referring to Figs. 11 and 12

m = 1.8 tons/in^2 and the initial shear flow stress

$(k - \frac{\Delta k}{2})$ = 29.0 tons/in^2

From Eqn. (18) γ = 2.41

From Eqn. (13) Δk = 4.35 tons/in^2

the shear flow stress, k, on AB is given by

$$k = \left(k - \frac{\Delta k}{2}\right) + \frac{\Delta k}{2}$$

$$= 31.2 \text{ tons/in}^2$$

From Eqn. (12) $p_{A/k} = 1.7$

From Eqn. (8) $(p_A - p_B)_{/k} = 1.4$

hence $p_{B/k} = .3$

from Eqn. (11) $\theta = 45°$

from Eqn. (19) $\lambda - \alpha = 20°$

For $\alpha = 10°$, $\lambda = 30°$, we can now say that the analysis gives $\phi = 25°$.

References

1. M.E. Merchant, 'Mechanics of Metal Cutting Process', Journal of Applied Physics, Vol. 16, 1945, p. 267.

2. H. Ll. D. Pugh, 'Mechanics of the Cutting Process', Proceedings, Conference on Technology of Engineering Manufacture, I.Mech.E., 1958.

3. J.M. Alexander and R.C. Brewer, 'Manufacturing Properties of Materials', Van Nostrand, 1963, p. 325.

4. P.L.B. Oxley and M.J.M. Welsh, 'Calculating the Shear Angle in Orthogonal Metal Cutting from Fundamental Stress-Strain Rate Properties of the Work Material', Proceedings 4th Int. M.T.D.R. Conference, 1963, p. 73.

5. W.B. Palmer and P.L.B. Oxley, 'Mechanics of Metal Cutting', Proceedings, I.Mech.E., Vol. 173, 1959, p. 623.

6. D. Kececioglu, 'Shear-Strain Rate in Metal Cutting and Its Effect on Shear Flow Stress', Trans. A.S.M.E., Vol. 80, 1958, p. 158.

7. K. Nakayama, 'A Study on the Mechanism of Metal Cutting', Journal of Soc. for Precision Mechanics, Vol. 23, 1957, p. 528.

8. H.E. Enahoro, Ph.D. Thesis, Sheffield University, 1964.

9. P.L.B. Oxley, 'Rates of Strain Effect in Metal Cutting'. Trans. A.S.M.E., Vol. 85, 1963, p. 335.

Captions to Figures

Fig. 1 Plastic Zone in Orthogonal Cutting
(a) cutting speed = $\frac{1}{2}$ in/min.
(b) cutting speed = 50 ft/min.

Fig. 2 Force Diagram.

Fig. 3 Shear Plane Model of Chip Formation.

Fig. 4 Merchant's Equations and Experimental Results.

Fig. 5 Merchant's Values for Shear Flow Stress and Hydrostatic Stress Calculated from Cutting Results.

Fig. 6 Shear Zone Model of Chip Formation.

Fig. 7 Shear Zone Element.

Fig. 8 Free Surface Element.

Fig. 9 Idealized Stress-Strain Curve

Fig. 10 Hodograph Showing Velocity Changes Across Shear Zone.

Fig. 11 Slope m - Shear Strain Rate Relation
———— Kececioglu's work material (SAE 1015)
- - - - - - - - Merchant's work material (NE 9445)

Fig. 12 Initial Shear Flow Stress - Shear Strain Rate Relation
———— Kececioglu's work material (SAE 1015)
---------- Merchant's work material (NE 9445)

Fig. 13 Variable Flow Stress Shear Angle Relations for Kececioglu's Work Material
———— 1 in/min.
---------- 1000 ft/min.

Fig. 14 Variable Flow Stress Shear Angle Relation For Merchant's Work Material and Cutting Conditions, with Experimental Results.

Fig. 15 Variable Flow Stress Values for Shear Flow Stress and Hydrostatic Stress for Merchant's Work Material and Cutting Conditions.

Fig. 16 Specific Cutting Pressure
(a) Calculated from Variable Flow Stress Theory ------ $\alpha = +10°$
———— $\alpha = -10°$
(b) Experimental Results ● $\alpha = +10°$
o $\alpha = -10°$

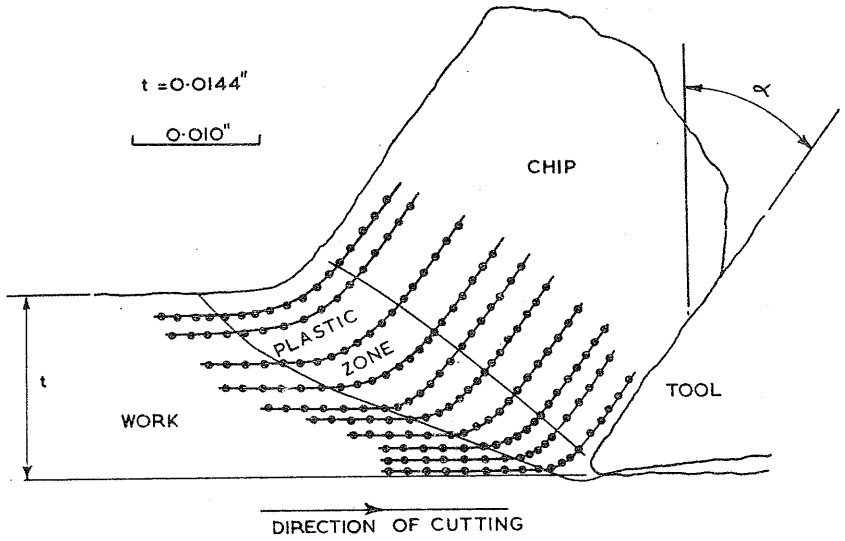

FIGURE 1(a)

(a)

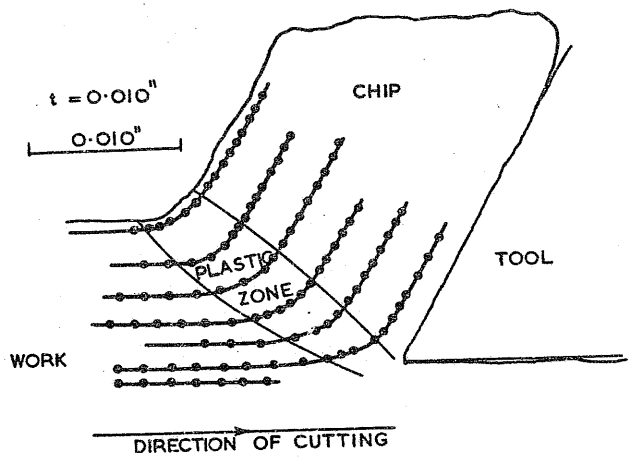

FIGURE 1(b)

(b)

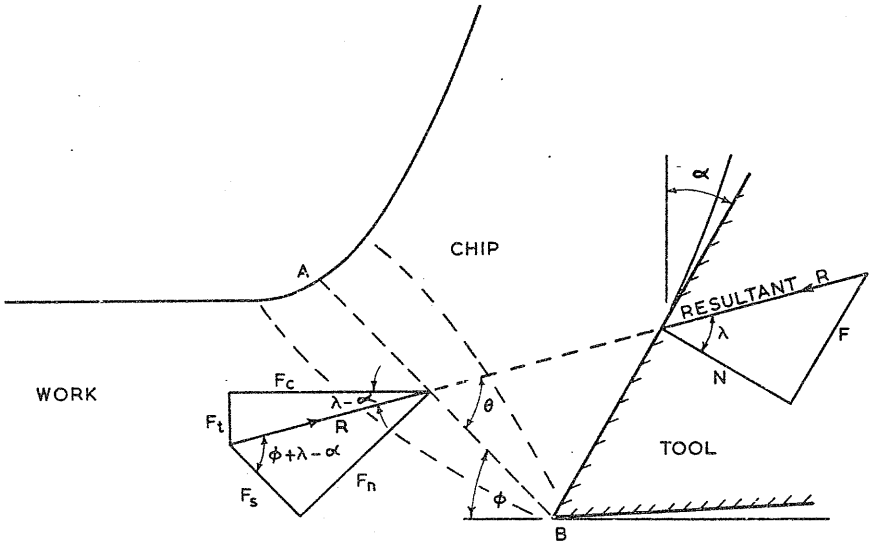

FIGURE 2

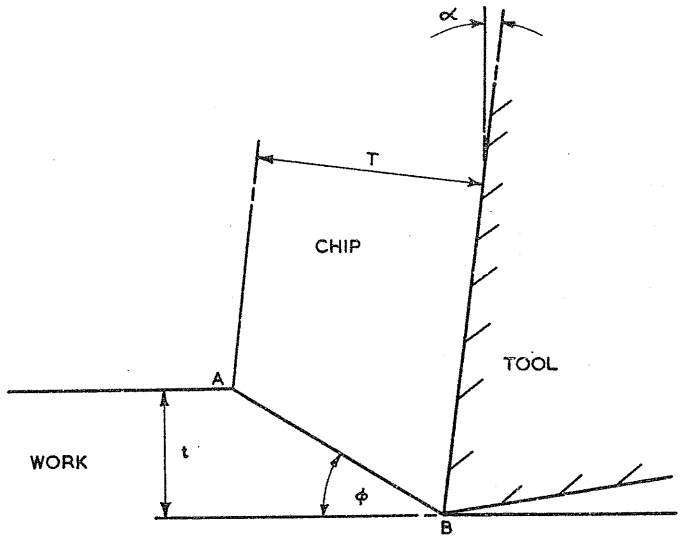

FIGURE 3

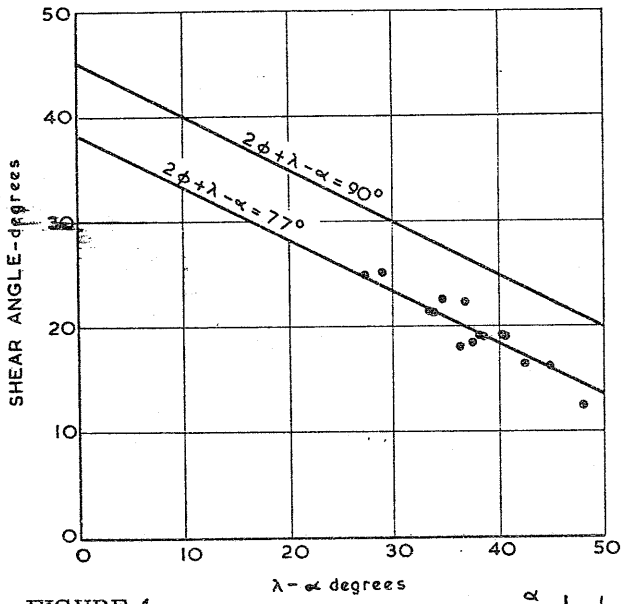

FIGURE 4

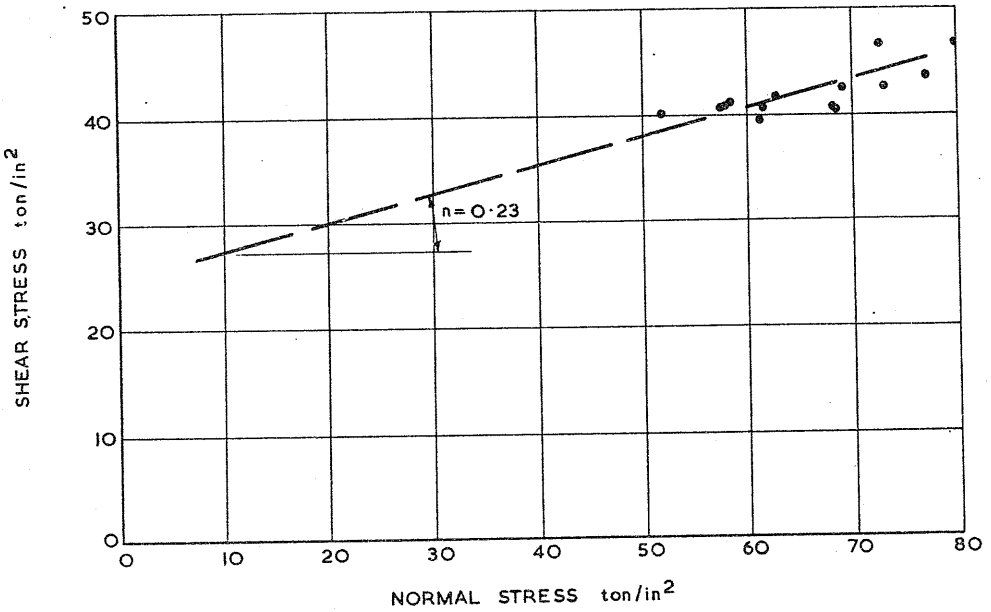

FIGURE 5

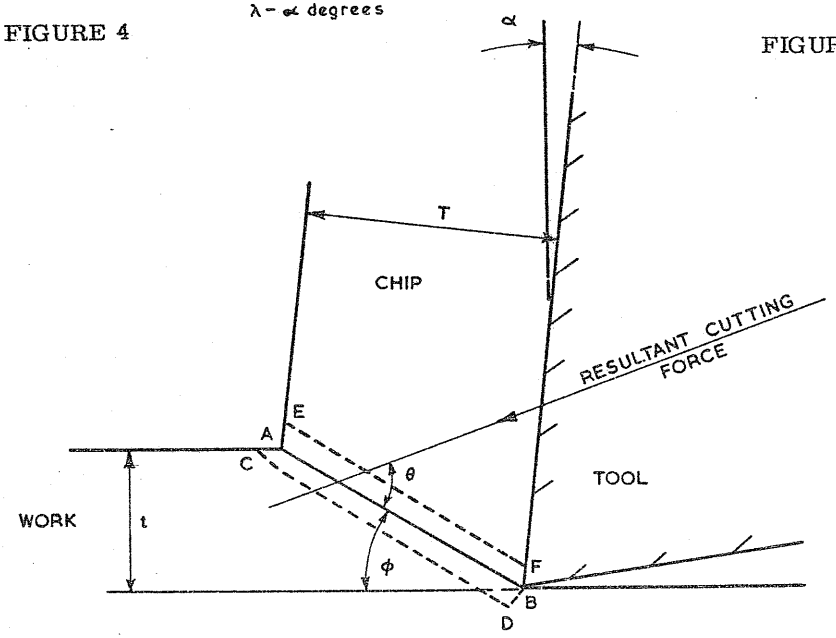

FIGURE 6

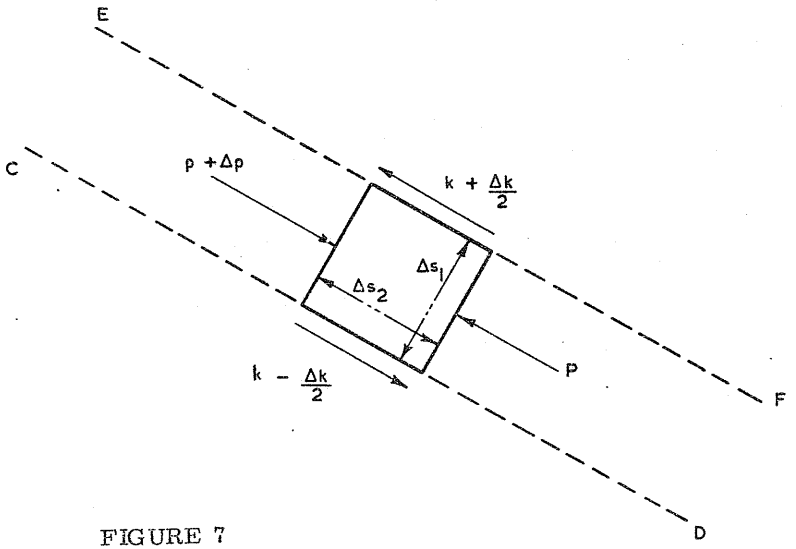

FIGURE 7

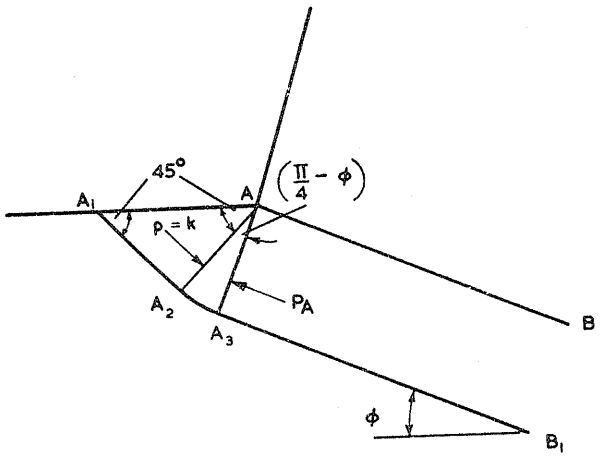

FIGURE 8

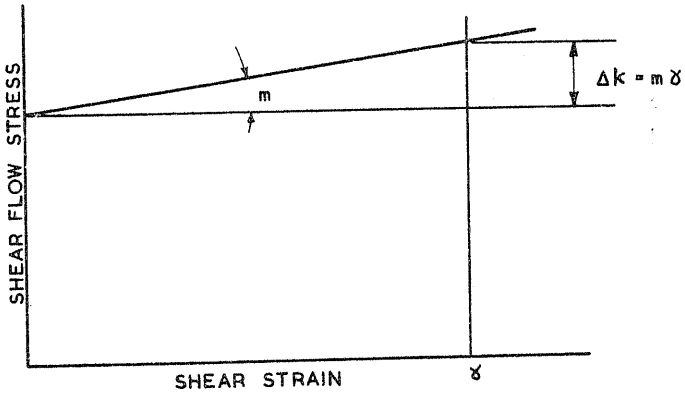

FIGURE 9

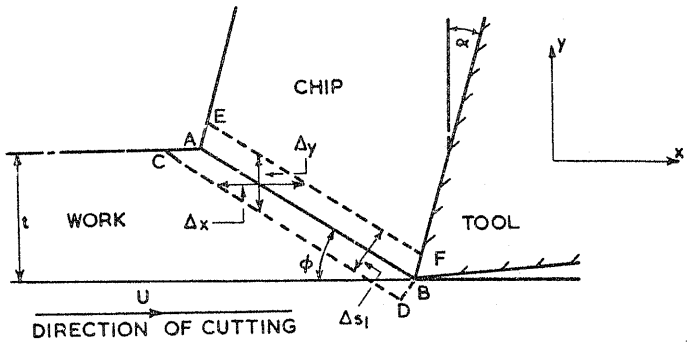

FIGURE 10

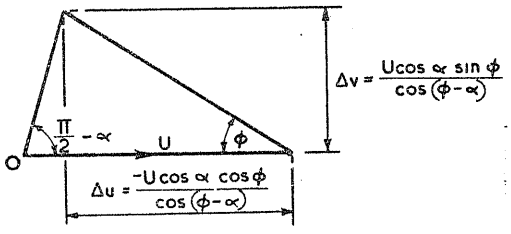

HODOGRAPH

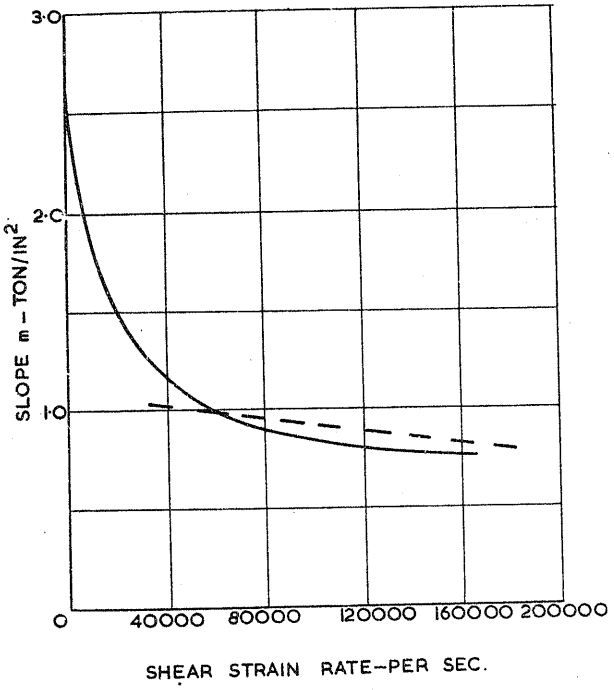

FIGURE 11

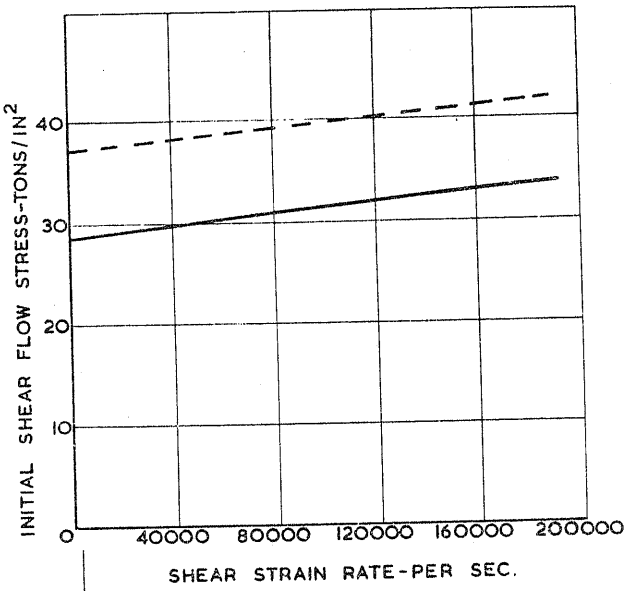

FIGURE 13

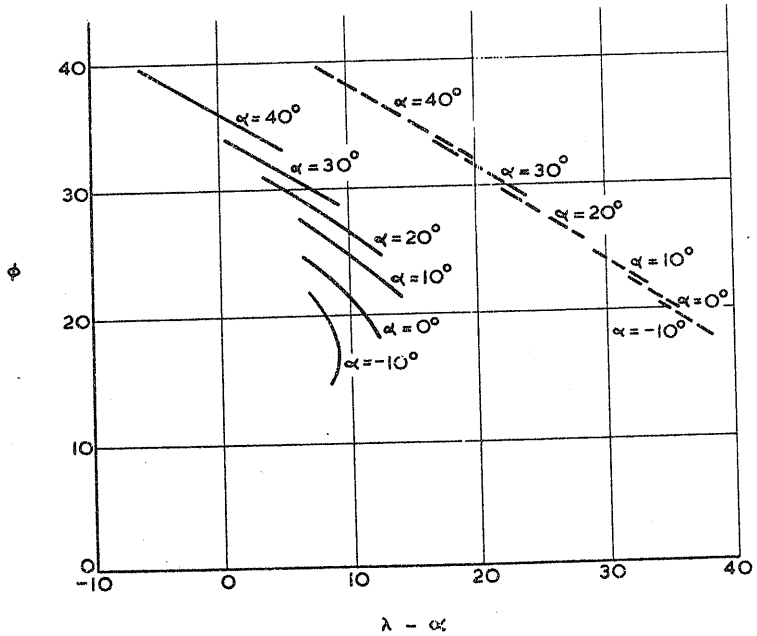

FIGURE 12

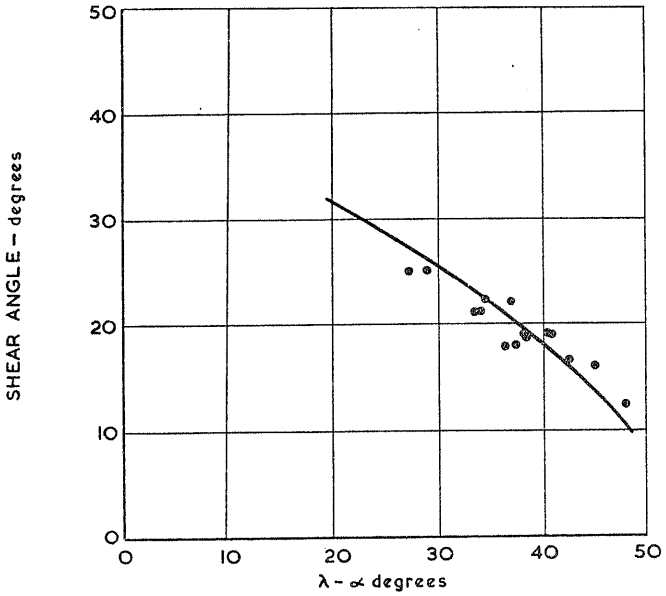

FIGURE 14

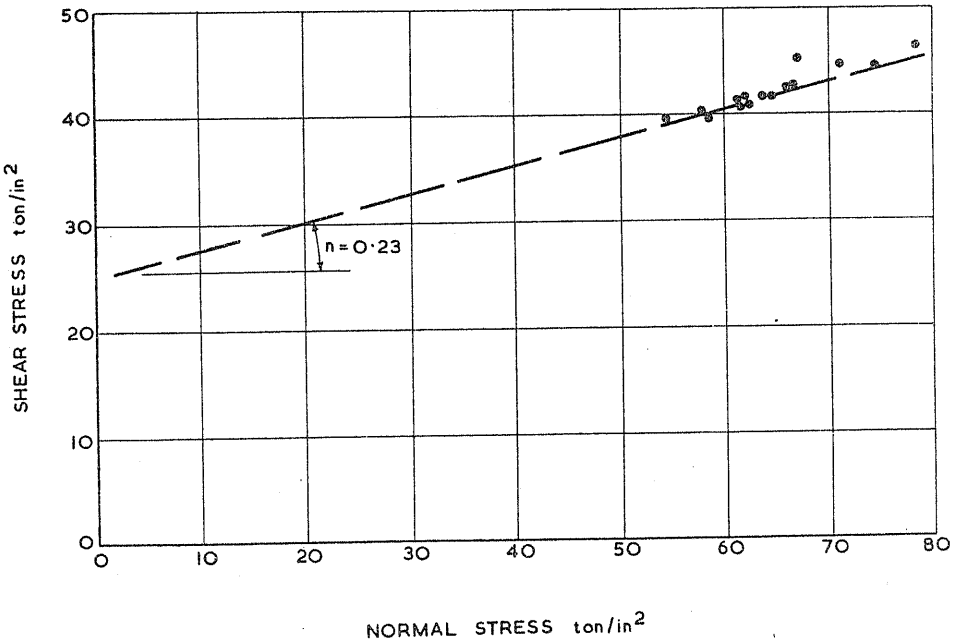

FIGURE 15

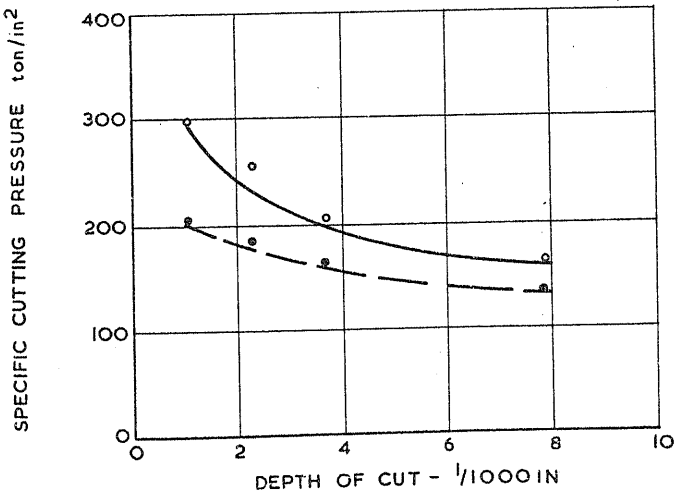

FIGURE 16